ELSEVIER

Journal of Neuroscience Methods 121 (2002) 111–127

JOURNAL OF NEUROSCIENCE METHODS

www.elsevier.com/locate/jneumeth

An efficient method for studying short-term plasticity with random impulse train stimuli

Ghassan Gholmieh [a], Spiros Courellis [a,*], Vasilis Marmarelis [a], Theodore Berger [a,b]

[a] *Department of Biomedical Engineering, OHE-500, mc-1451, University of Southern California, Los Angeles, CA 90089-1451, USA*
[b] *Neuroscience Program, University of Southern California, Los Angeles, CA 90089-2520, USA*

Received 12 December 2001; received in revised form 10 June 2002; accepted 10 June 2002

Abstract

In this article, we introduce an efficient method that models quantitatively nonlinear dynamics associated with short-term plasticity (STP) in biological neural systems. It is based on the Voterra–Wiener modeling approach adapted for special stimulus/response datasets. The stimuli are random impulse trains (RITs) of fixed amplitude and Poisson distributed, variable interimpulse intervals. The class of stimuli, we use can be viewed as a hybrid between the paired impulse approach (variable interimpulse interval between two input impulses) and the fixed frequency approach (impulses repeated at fixed intervals, varying in frequency from one stimulus dataset to the next). The responses are sequences of population spike amplitudes of variable size and are assumed to be contemporaneous with the corresponding impulses in the RITs they are evoked by. The nonlinear dynamics of the mechanisms underlying STP are captured by kernels used to create compact STP models with predictive capabilities. Compared to similar methods in the literature, the method presented in this article provides a comprehensive model of STP with considerable improvement in prediction accuracy and requires shorter experimental data collection time.

Keywords: CA1; Multielectrode array; Nonlinear analysis; Random impulse train; Short-term plasticity; Kernels

1. Introduction

Experimental studies investigating short-term plasticity (STP) use impulse sequence stimuli, as this type of signal comprises the most common form of input in biological neural systems. In particular, paired pulse stimulation of variable interimpulse intervals (Creager et al., 1980; Leung and Fu, 1994; Dobrunz et al., 1997) and short impulse trains at a fixed frequency (Yamamoto et al., 1980; Turner and Miller, 1982; Landfield et al., 1986; Abbot et al., 1997; Fueta et al., 1998; Pananceau et al., 1998), varying from one impulse train to another, have been used widely in experimental STP research. Each method identifies areas of facilitation and inhibition within the STP mechanisms only for a limited number of interimpulse intervals or impulse train frequencies. Using these methods, extension of the experimental protocol to cover a wide range of intervals and frequencies may prolong the experimental time to the point where the viability of the experimental preparation may not be viable or stable.

In this article, we present a new method to quantitatively describe STP in biological neural systems that uses impulse sequence stimuli of randomly variable interimpulse interval. The new method innovates in combining impulse sequence stimuli with quantitative STP descriptors derived using the Volterra–Wiener modeling approach (Wiener, 1958), adapted for impulse sequences of randomly varying interimpulse intervals at the input (Krausz and Friesen, 1975; Sclabassi et al., 1988). The output is the corresponding sequence of variable amplitude population spikes. Each population spike was recorded a short latency after the corresponding input impulse. Our choice of stimuli can be viewed as a hybrid of the variable interimpulse intervals used by the paired pulse approach and the pattern of repeated impulses at fixed intervals (with variable repetition rates from run to run) utilized by the fixed frequency approach.

* Corresponding author. Tel.: +1-213-740-0340; fax: +1-213-740-0343
E-mail address: shc@usc.edu (S. Courellis).

0165-0270/02/$ - see front matter
PII: S0165-0270(02)00164-4

The new approach leads to a comprehensive and compact representation of the nonlinear dynamics associated with STP in the form of a mathematical model. The latter comprises accurate STP descriptors (kernels) that are estimated from the input–output data and can be validated by means of their predictive capabilities for any input sequence. Compared to existing methods reported in the literature, the method presented in this article provides a compact representation of STP dynamics with considerable improvement in prediction accuracy and requires shorter experimental data collection time.

We have applied our method to the CA1 subregion of the hippocampus in vitro, since it has been a widely utilized experimental preparation (Andersen et al., 1971) in previous research for understanding STP (Creager et al., 1980; Leung and Fu, 1994), drug toxicity (Nelson et al., 1999; Alberston et al., 1996; Colmers et al., 1985), long-term potentiation (Bliss and Lomo, 1973; Harris and Teyler, 1983; Wheal et al., 1983; Harris et al., 1984), and genetic alterations (Krugers et al., 1997). However, the developed methodology is readily transferable to other hippocampal regions (e.g. Perforant Path–Dentate, mossy fibers-CA3) and to different biological preparations (e.g. midbrain and cortex).

This article is organized into sections on: (1) materials that describes the experimental setup; (2) methods that presents the data collection protocol and the data analysis approach; and (3) results that presents the obtained STP descriptors (kernels); outlines areas of facilitation and inhibition; describes the selection process of the estimation parameters; presents the use of empirically optimized impulse sequence stimuli with high interimpulse interval variability; presents validation results for the STP descriptors and demonstrates their predictive capabilities; and compares the proposed method with the cross-correlation approach (Berger et al., 1988a,b, 1989) for the estimation of the STP descriptors. Section 5 concludes the article, summarizing the experimental and computational improvements associated with the new method.

2. Materials

2.1. Biological preparations

Adult rats were completely anesthetized with Halothane and were decapitated. Their brain was extracted and transferred to a bath containing iced aCSF (128 mM NaCl, 2.5 mM KCl, 1.25 mM NaH_2PO_4, 26 mM $NaHCO_3$, 10 mM glucose, 2 mM $MgSO_4$, 2 mM ascorbic acid, 2 mM $CaCl_2$). The hippocampus was extracted and transverse slices (500 μm of thickness) were collected using a Leika vibrotome (VT 1000S). The slices were then left to equilibrate for 1 h in aCSF at room temperature.

2.2. Hardware

Extracellular recordings were achieved using a multielectrode array. The setup consisted of a multimicroelctrode plate (MMEP4, Gross et al., 1993; Univ. North Texas, www.cnns.org), pre-amplifiers, two data acquisition boards, and custom-developed software. The MMEP, a 64 electrode-array, designed in an 8×8 formation (MMEP 4 design), had an inter-electrode distance of 150 μm. Contacts at the periphery (32 from each side) were implemented using zebra strips. The signals were amplified $\times 2500$ in two stages. In the first stage, $\times 250$ amplification was achieved using custom-manufactured Plexon preamplifiers (www.plexoninc.-com). In the second stage, signals were amplified ($\times$ 10) and digitized using two data acquisition boards (Microstar; DAP 3200/214e series, http://www.mstar-labs.com), installed in parallel, in a PentiumII 450 MHz personal computer. The sampling interval was set at 136 μs (7.35 kHz) per channel. Except for the computer, the experimental setup was housed in a Faraday cage on an antivibration table.

2.3. Software

A customized user interface written in Matlab controlled the two data acquisition boards. Another user interface was developed for nonlinear analysis, allowing the simultaneous extraction and nonlinear analysis of the population spikes of four simultaneous recordings from four different channels.

3. Methods

3.1. Slice positioning

Each slice was positioned over the multielectrode array with the guidance of an inverted microscope (Leica DML $4\times$). The hippocampal slice was held down using a nylon mesh glued to a metallic ring. The slice, along with the metallic ring, was moved with a thin brush in order to position the CA1 cell body layer over a row of electrodes. Four electrodes near the cell body layer were selected for recording. A bipolar stimulation electrode (twisted Nichrome wires) was placed in the Schaffer collaterals region. After documenting the relative position of the slice with respect to the array (Fig. 1), using an analogue camera (Hitachi VK-C370), the slice was left for 15 min to equilibrate. The temperature was maintained at 30 °C.

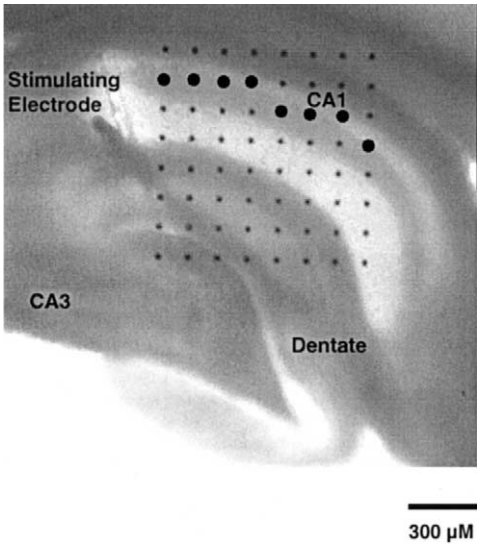

Fig. 1. Picture of a hippocampal slice positioned over the multi-electrode (8 × 8) array. Each black dot represents an electrode. The blackened electrodes show recording sites from CA1.

3.2. Random impulse train design

The CA1 population of neurons was stimulated with impulse trains (at 2 Hz average), whose interimpulse intervals followed a Poisson distribution. Such stimuli provide frequency rich sequences at a frequency range that does not cause LTP or LTD in pyramidal cells (Berger et al., 1988a; Perrett et al., 2001). A sequence of 4000 computer generated, Poisson distributed (2 Hz) intervals, were divided into 20 segments of 200 impulses each and were called random impulse trains (RITs).

3.3. Protocol of data collection

At the beginning of each experiment, an input–output curve was collected. The stimulation intensity for the rest of the experiment was set so that the population spike response would be at 10–30% of the maximum population spike response obtained via the IO curve (Berger et al., 1988b). Subsequently, twenty stimulation sequences were applied successively to the biological preparation. Each stimulation sequence consisted of a pair of pulses (pp) 30 ms apart, followed by a random impulse train (RIT) of 200 pulses (Poisson distributed interimpulse intervals with a mean of 2 Hz) 30 s later and 5 min of resting time. The interval between the beginning and the end of each stimulation sequence (paired pulse+RIT+5 min of resting time) was approximately 7 min.

The population spike amplitudes of the paired pulse evoked responses were used to evaluate the slice's electrophysiological stability. The experiment was discontinued if the response amplitude varied by more than ±20% from the baseline.

3.4. Data preprocessing

The data collected simultaneously from four different sites was analyzed off-line. The population spike amplitudes were extracted using the following rules based on a peak latency range of 4–11 ms: (1) when an electrical impulse within a random train was followed by another electrical impulse after 20 ms or more, the population spike amplitude was measured by taking the distance between the negative minimum and the corresponding midpoint on the line joining the two positive peaks; (2) when an electrical impulse within a random train was followed by another electrical impulse within 11–20 ms, the amplitude was measured by taking the difference between the first peak and the negative minimum; (3) when an electrical impulse within a random train was followed by another electrical impulse in less then 11 ms, the response for the first impulse was interpolated.

The population spike responses were checked for the quality of the waveform by visually evaluating five non-adjacent random train recordings. A recording was accepted for subsequent analysis if all the responses showed well-defined populations spikes overriding well-defined evoked postsynaptic potentials (Fig. 2). Since the latency was not taken into consideration, the population spike responses were considered to be contemporaneous with the stimulus occurrence and were represented as variable amplitude impulses (Fig. 3). The waveshape of the population spikes, which may vary considerably depending on the input sequence, was not part of our analysis.

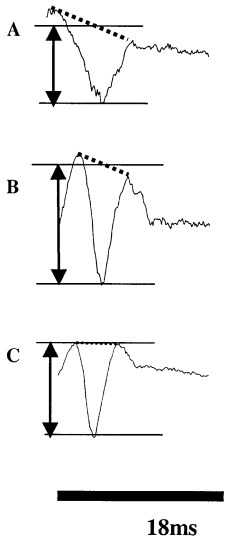

Fig. 2. Acceptable recorded waveforms: (A) acceptable waveform; (B) good waveform; (C) excellent waveform. A recording was accepted for subsequent analysis if the responses showed well-defined population spikes overriding well-defined evoked postsynaptic potentials. The population spike amplitude was measured by taking the distance between the negative minimum and the corresponding midpoint on the line joining the two positive peaks (line segments with arrows).

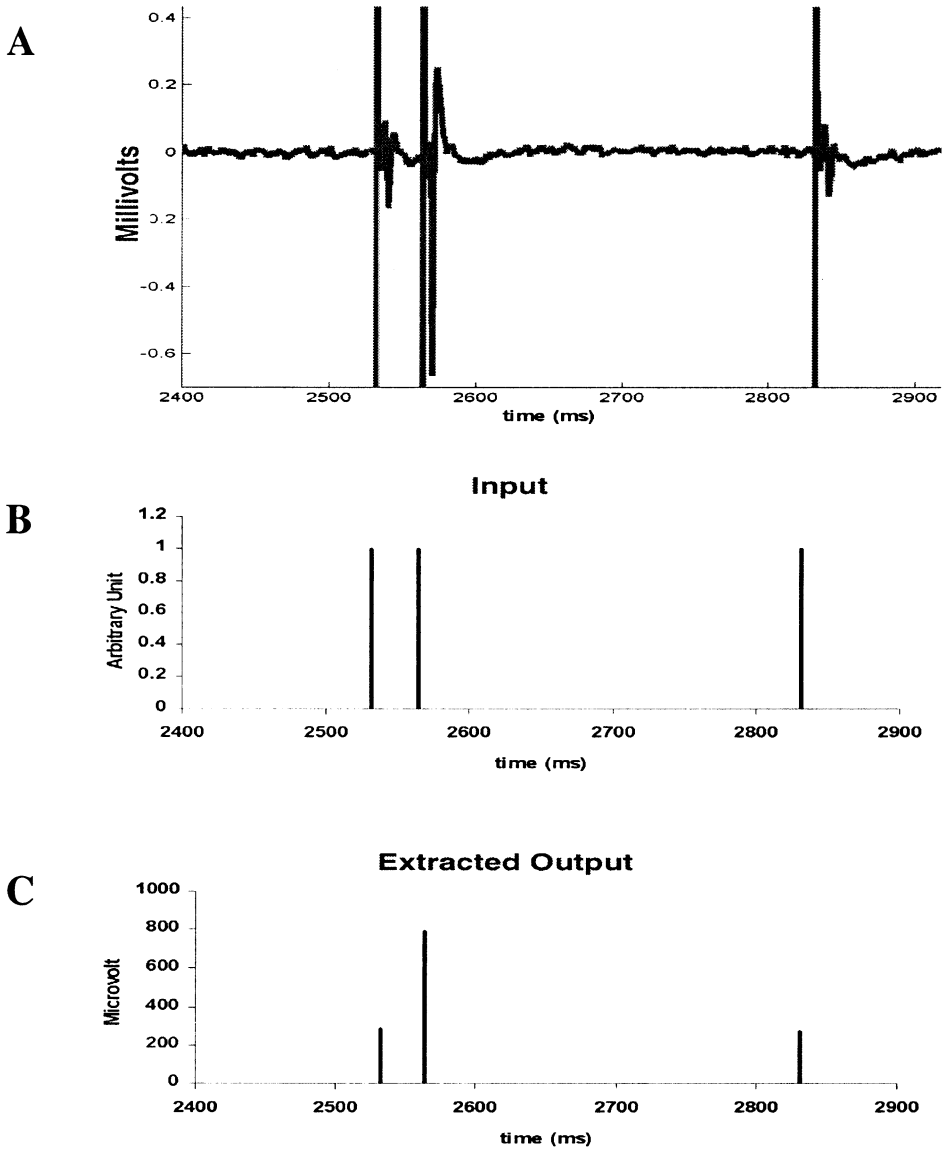

Fig. 3. Extraction of the population spike amplitude: (A) the stimulation artifact and the corresponding population spike waveform; (B) input aligned with the stimulus artifact; (C) extracted population spike amplitudes. Since the latency was not taken into consideration, the population spike responses were considered to be contemporaneous with stimulus occurrence and were represented as sharp spikes.

Recordings were checked for stability by plotting the mean of each response sequence against its number of occurrence during the recording. If the means of all the random train responses were within $\pm 15\%$ of the total mean, the data was saved for subsequent analysis (Fig. 4).

3.5. Analytical methods

The data was analyzed using a variant of the Volterra–Wiener approach adapted for fixed amplitude random impulse sequence stimuli and variable amplitude spike output sequences (Courellis et al., 2000). The adapted Volterra–Wiener approach considers the inter-impulse intervals as input and the amplitude of the population spikes as output. It also assumes that the population spike responses and the impulse stimuli that evoked them are contemporaneous. In our analysis, we employed the first- and second-order kernels, enabling us to construct the model shown in Eq. (1):

$$y(n_i) = k_1 + \sum_{n_i - \mu < n_j < n_i} k_2(n_i - n_j) \quad (1)$$

where n_i is the time of occurrence of the ith stimulus impulse and the corresponding response, n_j is the time of occurrence of the jth stimulus impulse preceding the ith stimulus impulse, $y(n_i)$ is the amplitude of the population spike in response to the impulse that occurred at time n_i, μ is the memory of the biological system, k_1 is the first-order kernel and k_2 is the second-order kernel.

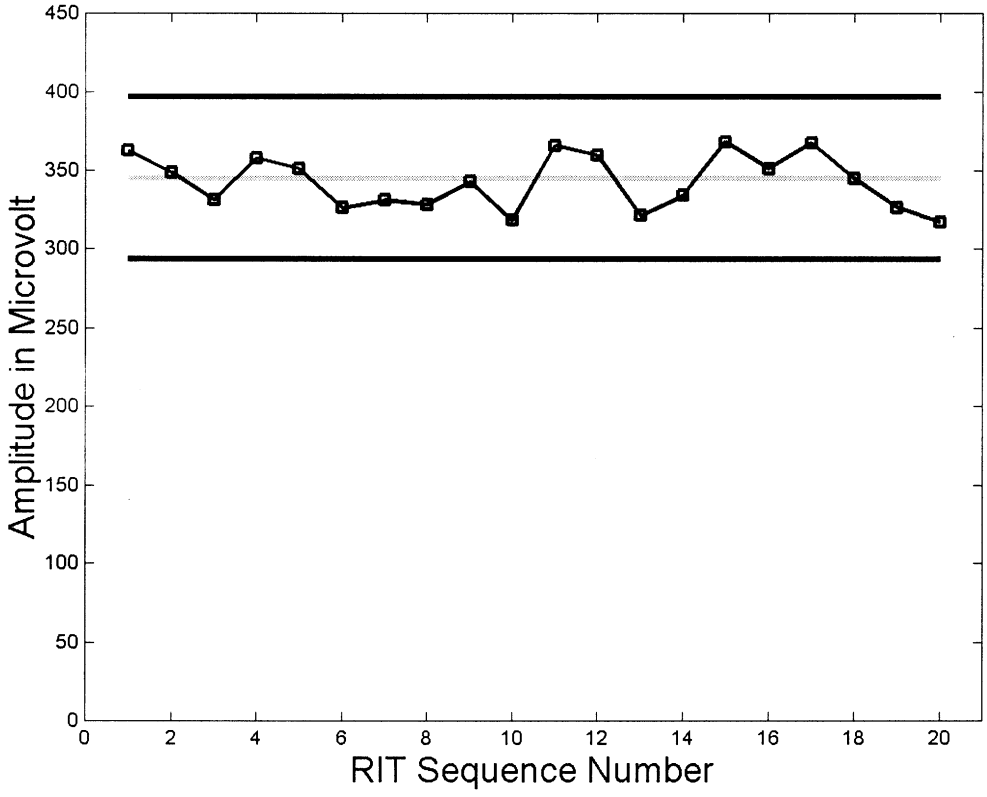

Fig. 4. Primary check for stability: each square represents the mean of the population spike amplitudes for each RIT (200 pulses) in the recording (20 RITs). If all mean values were within ±15% (outer black lines) of their average (middle line), the data was saved for subsequent analysis.

Eq. (1) describes the amplitude of the population spike at time (n_i) in terms of the first-order kernel (k_1) and the second-order kernel (k_2) at all values corresponding to time intervals from past impulses within the memory μ. The kernels, k_1 and k_2, capture the nonlinear dynamics of the underlying STP mechanisms and represent quantitative STP descriptors.

The first- and second-order kernels in the classical Volterra–Wiener sense are one- and two-dimensional functions respectively. In this article, the first-order kernel is a constant and the second-order kernel is a one-dimensional function. This is due to the fact that we do not consider variability in the latency between an impulse at the stimulus sequence and the population spike response evoked by it (Krausz and Friesen, 1975; Berger et al., 1988a; Sclabassi et al., 1988). The kernels in this case can be thought of as reduced order Poisson–Wiener kernels. The term 'reduced' is appropriate because of the reduced dimensionality of the kernels, the term 'Poisson' is used because the kernels are tied to a Poisson input, and the term 'Wiener' is included because the kernels are associated with an orthogonal functional expansion for Poisson inputs and are input dependent (i.e. different Poisson input mean rate parameters will yield different kernels, in general).

We used the Laguerre–Volterra method (Marmarelis, 1993) to estimate the kernels, an approach that reduces the kernel estimation effort to the computation of the coefficients of a set of Laguerre functions. The Laguerre basis functions form an orthonormal set and are defined as follows:

$$L_l(n) = \alpha^{(n-1)/2}(1-\alpha)^{1/2}\sum_{k=0}^{l}(-1)^k\binom{n}{k} \times \binom{l}{k}\alpha^{(l-k)}(1-\alpha)^k \quad (2)$$

where $L_l(\ )$ is the Laguerre basis function of lth order and alpha (α) is a parameter that varies between 0 and 1 and affects the time extent of the basis functions. The order of a Laguerre function corresponds to the number of times the function crosses the 'zero line'. Fig. 5A shows the 0th, 2nd, and 4th order Laguerre functions for a fixed value of alpha ($\alpha = 0.94$). Fig. 5B shows the 2nd order Laguerre functions for $\alpha = 0.90$, 0.94 and 0.95.

Using L Laguerre basis functions, the second order kernel can be expressed as:

$$k_2(n_i - n_j) = \sum_{l=0}^{L-1} c_l L_l(n_i - n_j) \quad (3)$$

where $L_l(\ )$ is the lth order Laguerre function and c_l is the corresponding expansion coefficient. Combining Eqs. (1) and (3), we obtain:

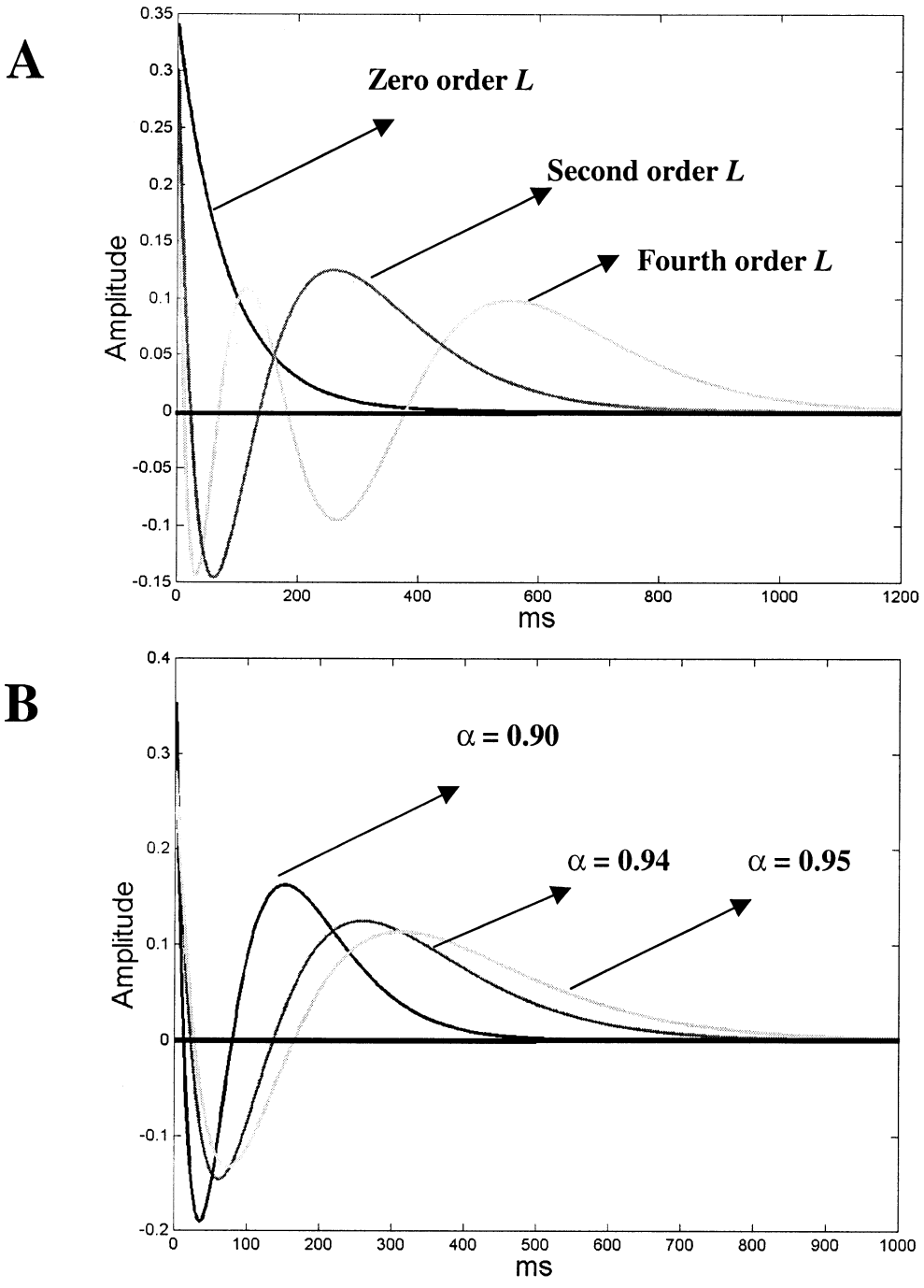

Fig. 5. Example of Laguerre basis functions: (A) 0th, 2nd and 4th order Laguerre functions for $\alpha = 0.94$. The order of the function correlates with the number of times it crosses the zero line. (B) The 2nd order Laguerre function for different values of alpha ($\alpha = 0.90, 0.94, 95$). As alpha increases, the time extent of the Laguerre functions increases.

$$\left\{ y(n_i) = k_1 + \sum_{n_i - \mu < n_j < n_i} \sum_{l=0}^{L-1} c_l L_l(n_i - n_j) \right\}_{i=1,\ldots,\ N} \tag{4}$$

Since c_l are constant, Eq. (4) can be rearranged as follows:

$$\left\{ y(n_i) = k_1 + \sum_{l} c_l \sum_{n_i - \mu < n_j < n_i} L_l(n_i - n_j) \right\}_{i=1,\ldots,\ N} \tag{5}$$

Eq. (5) applies to every population spike amplitude $[y(n_i)]$ in the dataset. The first-order kernel (k_1) and the Laguerre coefficients (c_l) are calculated using the min of least squares error on the set of N equations expressed by Eq. (5). For example, 4000 equations are formed using all twenty RITs in order to calculate the value of k_1 and the Laguerre coefficients (c_l) that lead to the estimation of k_2 using Eq. (3).

The kernel estimates can be interpreted as follows: the first-order kernel can be interpreted as the mean of the population spike amplitude, while the second-order kernel represents the effect of the interaction between the current impulse stimulus and past stimulus impulses (within a memory window μ) on the amplitude of the current population spike (facilitation for positive values and inhibition for negative values). The role of the first- and second-order kernel in the model shown in Eq. (1) is illustrated in Fig. 6. The first-order kernel contributes a constant value to the model response and the second-order kernel provides the requisite amplitude adjustment, based on the time interval between the current impulse and past impulses that occurred within a memory window μ. Throughout this article, we have normalized the values of the second-order kernels by dividing them with the corresponding value of the first-order kernels. Thus, second-order kernels represent percentage adjustments with respect to the first-order kernel.

The predictive accuracy of the estimated kernels is evaluated using the normalized mean square error (NMSE), defined as follows:

$$\mathrm{NMSE} = \frac{\sum_i (Y_{\mathrm{pr}} - Y_{\mathrm{data}_i})^2}{\sum_i Y_{\mathrm{data}_i}^2} \tag{6}$$

where Y_{pr} is the predicted amplitude of the population spikes using the estimated kernels and Y_{data} is the actual amplitude extracted from the recorded data. The NMSE is a measure of how well kernels can capture the system nonlinear dynamics. If the NMSE value is small, the kernels model the biological system very well. If the NMSE value is large, either the quantitative model requires higher order terms (kernels) to be included or the data are noisy and/or unreliable.

In establishing a measure of comparison with existing methods, we employed the cross-correlation method for kernel estimation (Krausz and Friesen, 1975; Berger et

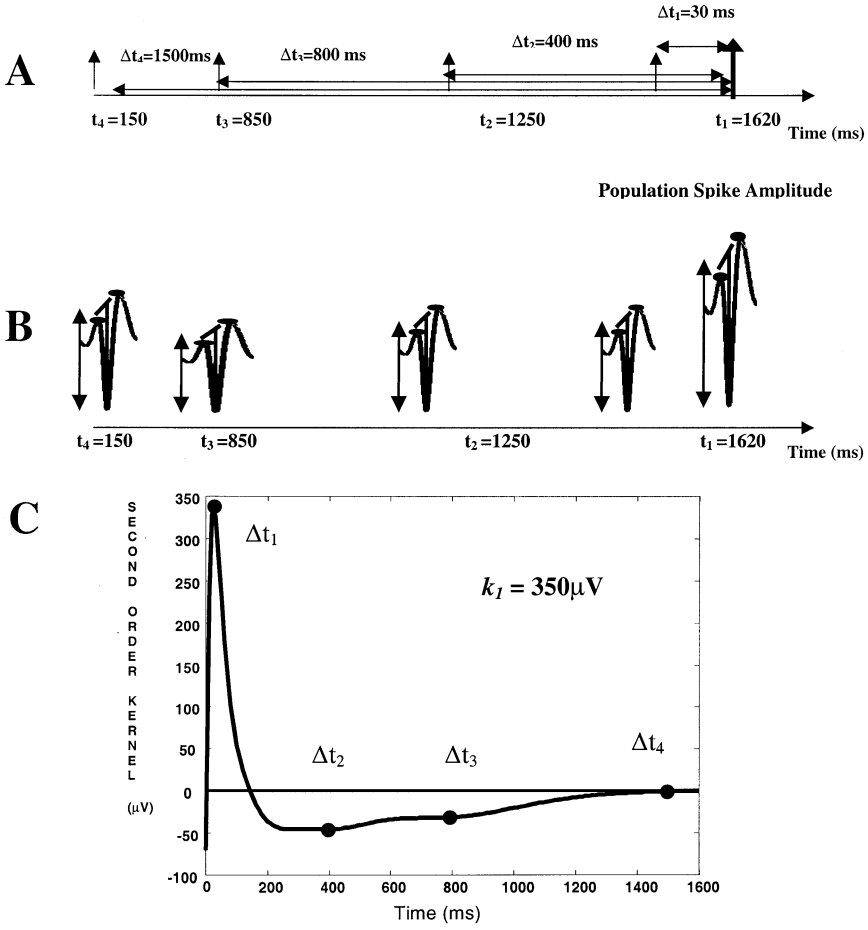

Fig. 6. Predictive power of the kernels. (A) A series of input electrical stimuli applied through a stimulating electrode to the Schaffer Collaterals where ?t indicate the time difference between the present impulse and the past impulses. (B) The corresponding recorded population spikes. The amplitude of each population spike was measured as the difference of the distance between the population spike minimum and the midpoint of the line that joins the two positive peaks. (C) The first- and second-order kernel. The amplitude of the response for the last impulse (bold arrow, at 1650 ms) can be estimated using the first-order kernel, the second-order kernel, and Eq. (1) as follows: $y(1650) = k_1 + k_2(1650-1620) + k_2(1650-1250) + k_2(1650-850) + k_2(1650-150) = k_1 + k_2(?t_1) + k_2(?t_2) + k_2(?t_3) + k_2(?t_4) = k_1 + k_2(30) + k_2(400) + k_2(800) + k_2(1500) = 350 + 340 - 30 - 30 + 0 = 630$ μV.

al., 1988a; Sclabassi et al., 1988). The resulting kernels were compared to kernels obtained using the presented approach.

4. Results

The experimental effort consisted of six experiments, including four simultaneous recordings from each experiment, a total of 24 recordings. Each recording was comprised of population spike responses to twenty stimulus sequences. Each stimulus sequence was formed by combining one pulse pair, one RIT (a sequence of fixed amplitude impulses, whose interimpulse interval followed a Poisson distribution), and 5 min of resting time. We used the adapted Volterra–Wiener method to analyze the STP nonlinear dynamic characteristics captured by the estimated kernels.

4.1. Determining the estimation parameters (L and alpha) for the adapted Volterra–Wiener approach

The number of the Laguerre basis functions L (Eq. (3)) and the value of the parameter alpha (α) for estimating the kernels were chosen to minimize the NMSE. Fig. 7A shows the NMSE associated with one recording, plotted over a range of α values between 0.7 and 0.99, and for $L = 5$, 7, 9, 11 Laguerre basis functions. The choice of $L = 9$ and $\alpha = 0.93$ provided optimal kernel estimates resulting in a NMSE of 3.6%. Fig. 7B shows first- and second-order kernels for $\alpha = 0.93$ and $L = 5$, 7, 9. The first-order kernel (k_1, mean population spike) fluctuated only within 5%, while second-order kernels (k_2) exhibited an initial rising phase, followed by a fast relaxation phase, and crossed into a shallow inhibitory phase shortly after 100 ms. Variation in the number of the Laguerre functions L and the parameter alpha affected mainly the inhibitory phase, extending its duration as L and alpha increased (e.g. Fig. 7B). A plot of the Laguerre coefficients values for $\alpha = 0.93$ shown in Fig. 7C confirmed that $L = 9$ is a good choice, as the value of the Laguerre coefficients becomes negligible for $L > 9$.

Results from the analysis of two more recordings are shown in Fig. 8. Fig. 8B,D show NMSE curves plotted over α for $L = 5$, 7, 9, 11. The choice of $L = 9$ still minimizes NMSE. The minimum NMSE value of 4.8% occurred at $\alpha = 0.93$ for the first recording (Fig. 8B) and the minimum NMSE value of 9% occurred at $\alpha = 0.94$ for the second recording (Fig. 8D). The corresponding kernel estimates for $L = 9$ are shown in Fig. 8A,C respectively. Using $L = 9$ and the same range of α, we computed kernels based on datasets from simultaneous recordings of four output channels (Fig. 9). The associated NMSE values were 1.36% for channel 20, 2.23% for channel 21, 1.71% for channel 22, and 2.56% for channel 26.

Across all the recordings, the NMSE was in the range of 1–9% suggesting the potential for a third-order kernel. Alpha had a mean value of 0.93 and a standard deviation of ± 0.01. Fig. 10 shows the mean and the variability of each Laguerre coefficient across all twenty-four recordings, normalized to the peak facilitation of the second-order kernel. It can be readily inferred that all the computed second-order kernels from all the recordings have approximately the same shape. In particular, the second-order kernels (describing STP nonlinear dynamics), exhibited a facilitation peak between 25 and 35 ms, a fast rising phase [0–30 ms] before the peak, and a fast facilitatory relaxation phase after the peak, crossing to the inhibitory region around 100–120 ms and returning to the baseline within 1600–2000 ms (memory extent), i.e. impulses that occurred after the return to the baseline had no effect on the amplitude of the population spike evoked by the present impulse. These results confirm that $L = 9$ and $0.92 < \alpha < 0.94$ lead to good kernel estimates.

4.2. Empirical optimization of the stimulus train

In each recording, the stimulus sequence included twenty independent RITs of 200 pulses each, resulting in long recording periods that impacted the viability of the experimental preparation and increased the computational burden of estimating the kernels. To address this issue, we tried to empirically explore the use of a subset of RITs leading to shorter stimulus sequences while maintaining the quality of the kernel estimates across all recordings.

We exhaustively searched various RIT combinations and found that two RITs (namely RIT #5 and RIT #11) were sufficient to form a stimulus sequence, which yielded first- and second-order kernel estimates comparable to the ones obtained with twenty RITs. In Fig. 11, kernels obtained using the two RITs are compared with kernels obtained from all twenty RITs using the proximity of k_1 and k_2 values and the respective NMSE curves. Fig. 11A, C and E show the first- and second-order kernels obtained from three recordings using all twenty RITs (black) and their counterparts using only RIT #5 and RIT #11 (gray). The proximity exhibited by k_1 values was within 5% and the visual assessment between corresponding second-order kernels revealed very strong similarities. Moreover, the correlation coefficient between k_2 values (> 0.99) confirmed the strong similarity between the estimated second-order kernels using all twenty RITs and the second-order kernel estimates using only RITs #5 and #11. Finally, the NMSE curves corresponding to RITs #5 and #11 shown in Fig. 11B, D and F are comparable to the ones corresponding to all 20 RITs depicted in Figs. 7A and

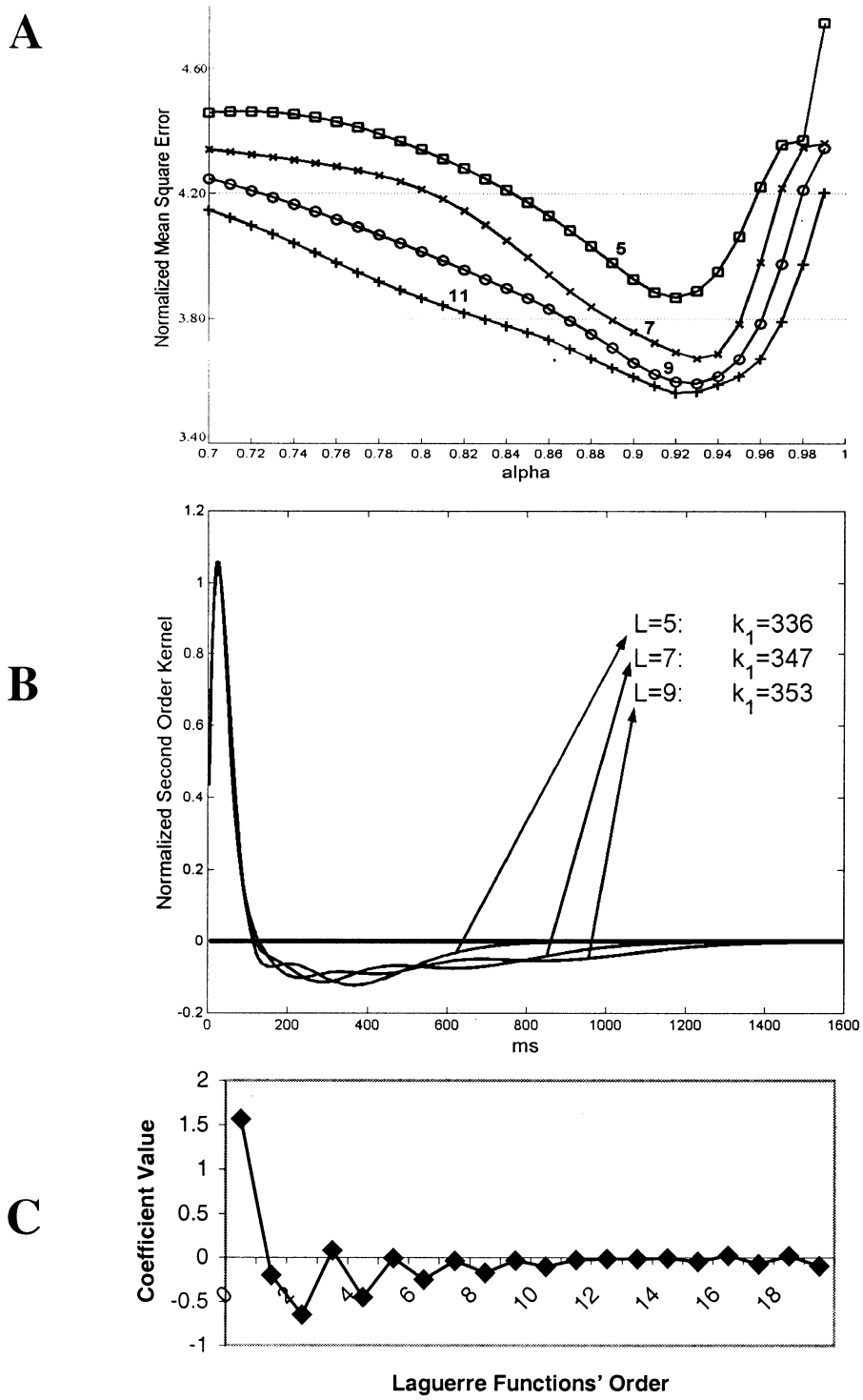

Fig. 7. Determination of the number of Laguerre basis functions L and the range of the alpha (α) parameter: (A) NMSE, associated with one recording, plotted over a range of α values between 0.7 and 0.99, and for $L = 5(\square),7(\times),9(\bigcirc),11(+)$. The choice of $L = 9$ and $\alpha = 0.93$ provided kernel estimates resulting in a NMSE of 3.60%. (B) First- and second-order kernel estimates for $L = 5$, 7 and 9. The estimated mean population spike k_1 (first-order kernel) fluctuated only by 5%. The estimated second-order kernels exhibited an initial rising phase, followed by a fast relaxation phase, and a shallow inhibitory phase. Variation in the number of the Laguerre functions L affected mainly the inhibitory phase, extending its duration as L increased. (C) A plot of the Laguerre coefficient values for $L = 21$ and $\alpha = 0.93$. It confirms that $L = 9$ is a good choice, as the values of the coefficients become insignificant for $L > 9$.

8B,D and provide a NMSE minimum of less then 4.41% at $L = 9$.

The assessment criteria confirmed that, in our case, the two RITs (namely #5 and #11) were adequate to

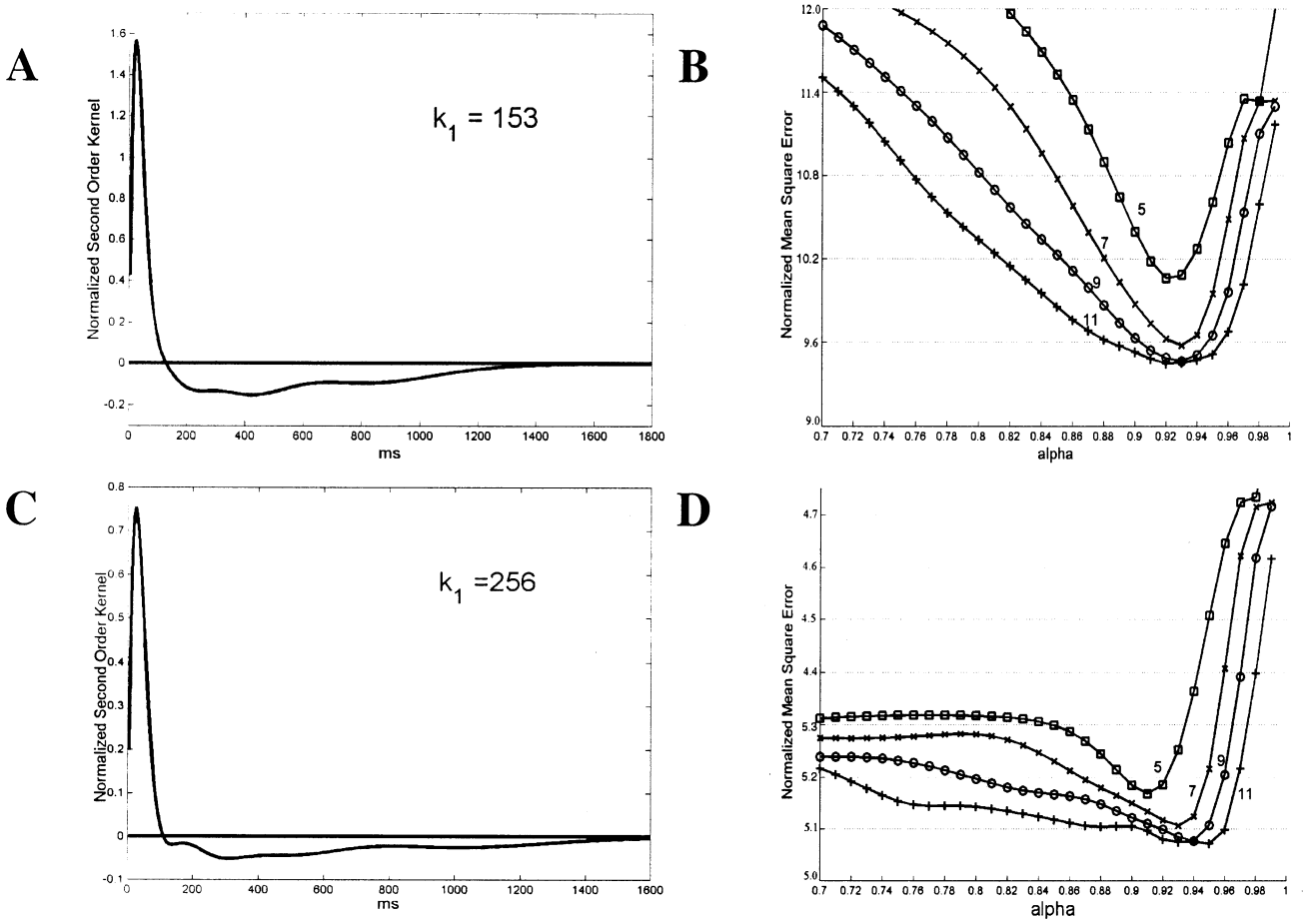

Fig. 8. Analysis of two more recordings: (B) and (D) show the NMSE curves plotted over α and parameterized in L. The choice of $L = 9$ and $\alpha =$ 0.93 and 0.94, respectively, leads to good kernel estimates and NMSE of 9.61 and 5.16% respectively. (A) and (C) show the corresponding first- and second-order kernels.

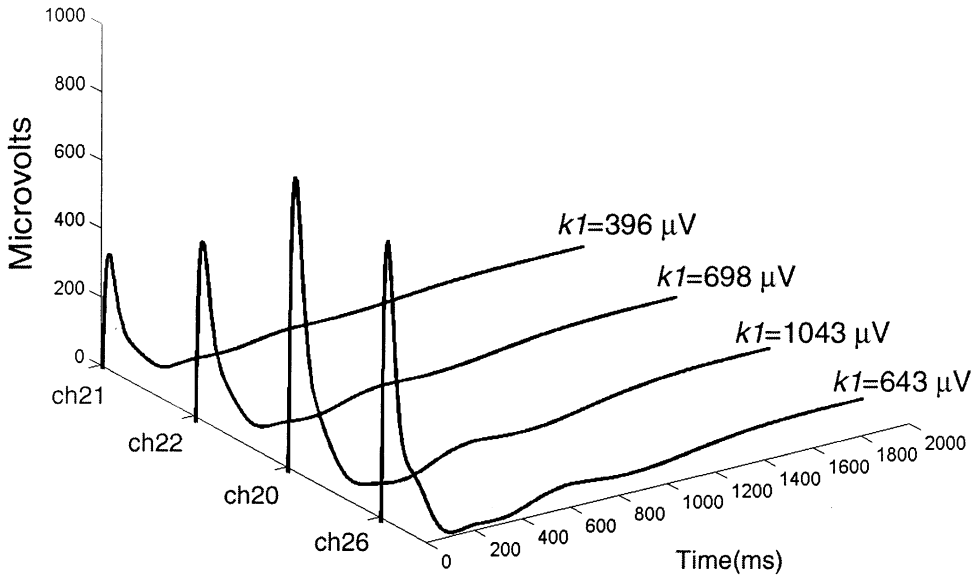

Fig. 9. Computed kernels based on datasets from simultaneous recordings of four output channels. The associated NMSE values were 1.36% for channel 20, 2.23% for channel 21, 1.71% for channel 22, and 2.56% for channel 26.

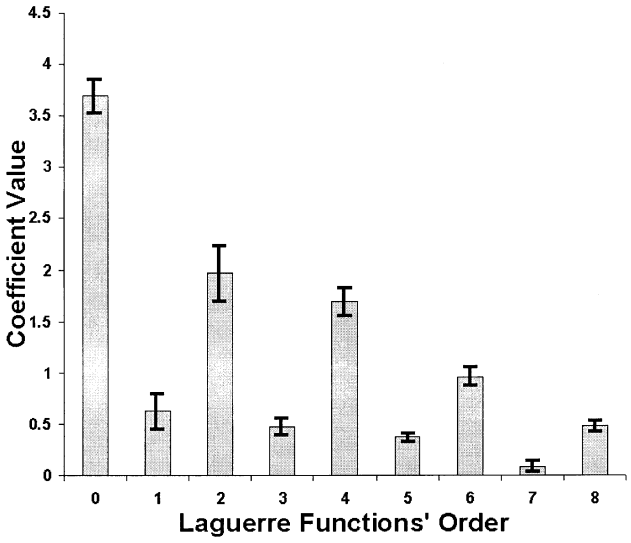

Fig. 10. The mean and variability of each Laguerre coefficient across all the recordings normalized to the peak facilitation of the second-order kernel. It can be readily inferred that all the computed second-order kernels from all the recordings have approximately the same shape and that the choice of $L = 9$ is suitable since the coefficient values become low beyond the sixth coefficient (error bars represent $\pm$ S.D.).

estimate the nonlinear dynamics of the biological system under study using the adapted Volterra–Wiener approach. This empirical optimization reduced the required number of RITs, in our case, by a tenfold and decreased the experimental time from 2 h to approximately 5 min. Finally, we computed the histograms of the interimpulse intervals of the various RIT combinations we tested and observed that the histogram of the interimpulse intervals of RITs #5 and #11 spanned the system memory more densely than the histograms of other RIT combinations. In general, one could empirically determine combinations of RITs suitable for their case by trying various RIT combinations and applying the assessment criteria presented earlier in this section.

4.3. Predictive power of the STP descriptors

In addition to providing a quantitative description of the nonlinear dynamics of the underlying STP, the kernels have predictive capabilities when used in conjunction with the STP model of Eq. (1). The STP model's (Eq. (1)) predictive capabilities are illustrated in Fig. 12. Fig. 12A,B show in-sample prediction while Fig. 12C shows out-of-sample prediction.

Fig. 12A shows a segment of population spike amplitudes (black squares) taken from RIT #11 and the corresponding model prediction (overlaid gray circles). The predicted output was estimated using first- and second-order kernels that were calculated from all the 20 input–output datasets and the associated NMSE value was 1.83%. Fig. 12B shows the same response data segment (black squares) predicted using first- and second-order kernels estimated from the empirically optimized dataset corresponding to RITs #5 and #11 (gray circles). In this case, the NMSE value was 1.37%. Comparison between Fig. 12A,B, and the associated NMSE values illustrates the predictive quality of the STP model in the case of non-optimized and optimized stimulus, respectively.

The predictive power can be fully illustrated using out-of-sample prediction where the system output for a stimulus dataset is predicted using kernels from a different input/output dataset. Fig. 12C shows a segment of real data that belonged to RIT #15 (black squares). The predicted output (gray circles) was estimated using first- and second-order kernel estimates using the input/output datasets corresponding to RIT #5 and RIT #11. Visual assessment and the computed NSME value of 4% illustrate the predictive power of the kernels characterizing STP in the CA1 hippocampal subsystem.

The STP model defined by Eq. (1) and the computed kernels can also be used to estimate the population spike amplitude of the conditioned response in paired impulse experiments and the amplitudes of population spike responses in fixed frequency experiments. In the case of paired impulse stimuli, the conditioned response $y_{\text{cond}}(\Delta)$ can be estimated, using Eq. (1), as follows:

$$y_{\text{cond}} = k_1 + k_2(\Delta) \tag{7}$$

where Δ is the interimpulse interval between the two stimulus impulses, k_1 is the computed first-order kernel, and k_2 is the computed second-order kernel. Dividing both sides of Eq. (8) by k_1, we obtain the normalized conditioned response $\tilde{y}_{\text{cond}}$:

$$\tilde{y}_{\text{cond}} = 1 + \frac{k_2(\Delta)}{k_1} \tag{8}$$

Using kernels computed previously and Eq. (8), we obtained estimates of the conditioned response shown in Fig. 13 for interimpulse intervals varying from 0 to 2000 ms. Fig. 13 suggests facilitatory behavior for interimpulse intervals between 0 and 200 ms and inhibitory behavior for interimpulse intervals between 200 and 2000 ms. In the literature, research findings have typically revealed facilitatory behavior for all interimpulse intervals (e.g. Dobrunz et al., 1997; Leung and Fu, 1994; Creager et al., 1980), but there are papers that have reported facilitatory behavior followed by inhibitory behavior (e.g. Stanford et al., 1995). The predictions shown in Fig. 13 are based on computed kernels from RIT stimuli and have not been validated with data from paired impulse experiments yet.

In the case of fixed frequency impulse train stimuli, the amplitude of the rth population spike response can be estimated, using Eq. (1), as follows:

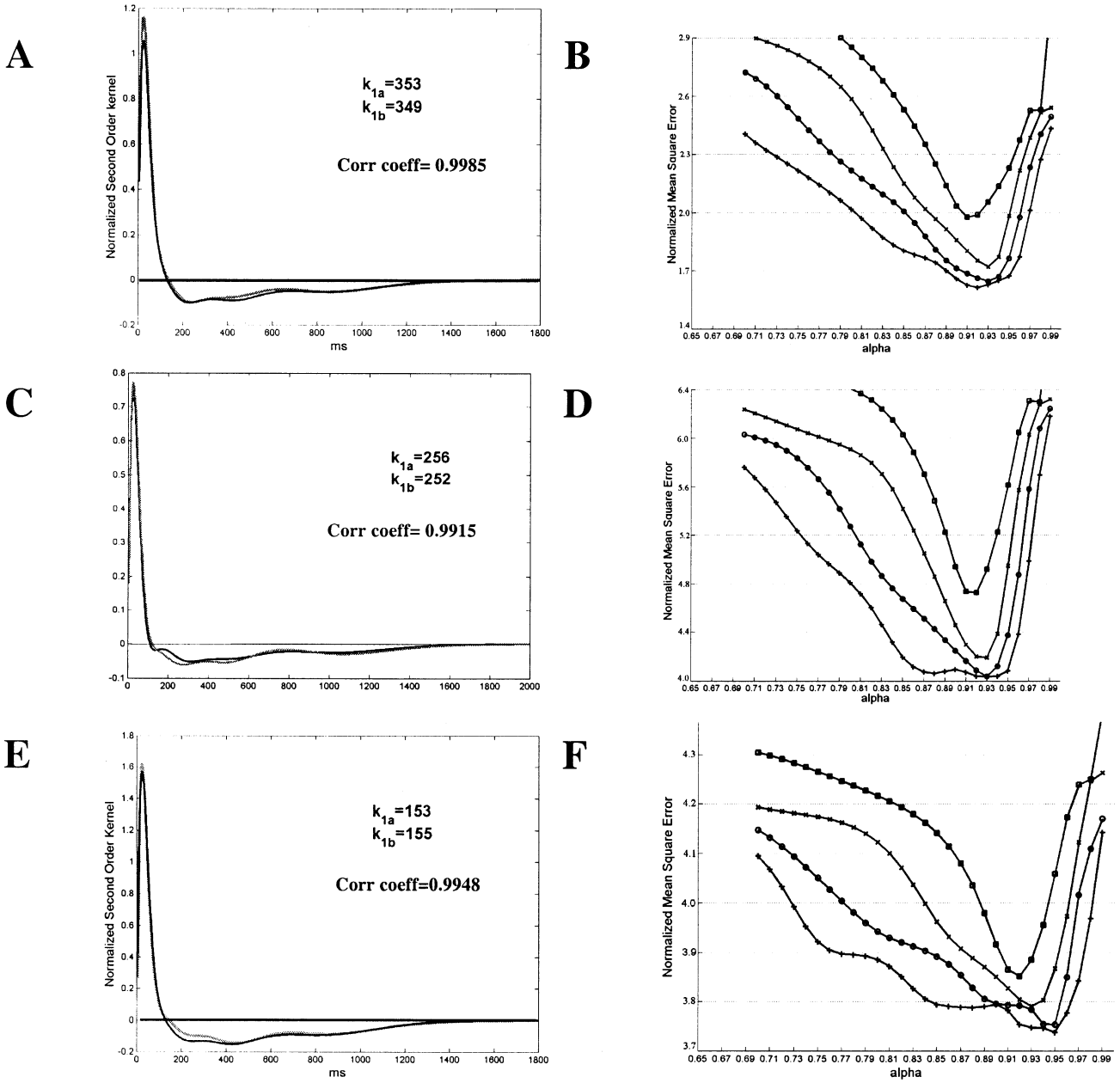

Fig. 11. Kernels estimated using the empirically optimized stimulus sequence and their corresponding NMSE plots. (A), (C) and (E) show the first- and second-order kernels obtained using the twenty RITs (k_{1a}, black trace) and their counterparts using only RIT #5 and RIT #11 (k_{1b}, gray trace). (B), (D) and (F) show the corresponding NMSE curves. Visual assessment, NMSE values ($<4.41\%$), and the correlation coefficient (>0.99) support the strong similarity between the estimated kernels using all twenty RITs and the kernel estimates using only RITs #5 and #11.

$$y_r = k_1 + \sum_{\rho=1}^{r} k_2(\rho\Delta) \tag{9}$$

$$\tilde{y}_r = 1 + \sum_{\rho=1}^{r} \frac{k_2(\rho\Delta)}{k_1} \tag{10}$$

where Δ is the interimpulse interval between successive spikes in the impulse train stimulus, k_1 is the computed first-order kernel, and k_2 is the computed first-order kernel. Dividing both sides of Eq. (9) by k_1, we obtain the normalized response $\tilde{y}_r$:

Using kernels computed previously and Eq. (10), we obtained estimates of the amplitude of the population spike response to the 2nd, 3rd, 4th, 5th and 6th impulse (Fig. 14) for interimpulse intervals of 50, 75 and 100 ms. Fig. 14 suggests facilitatory behavior (population spike amplitudes greater than one), an observation consistent

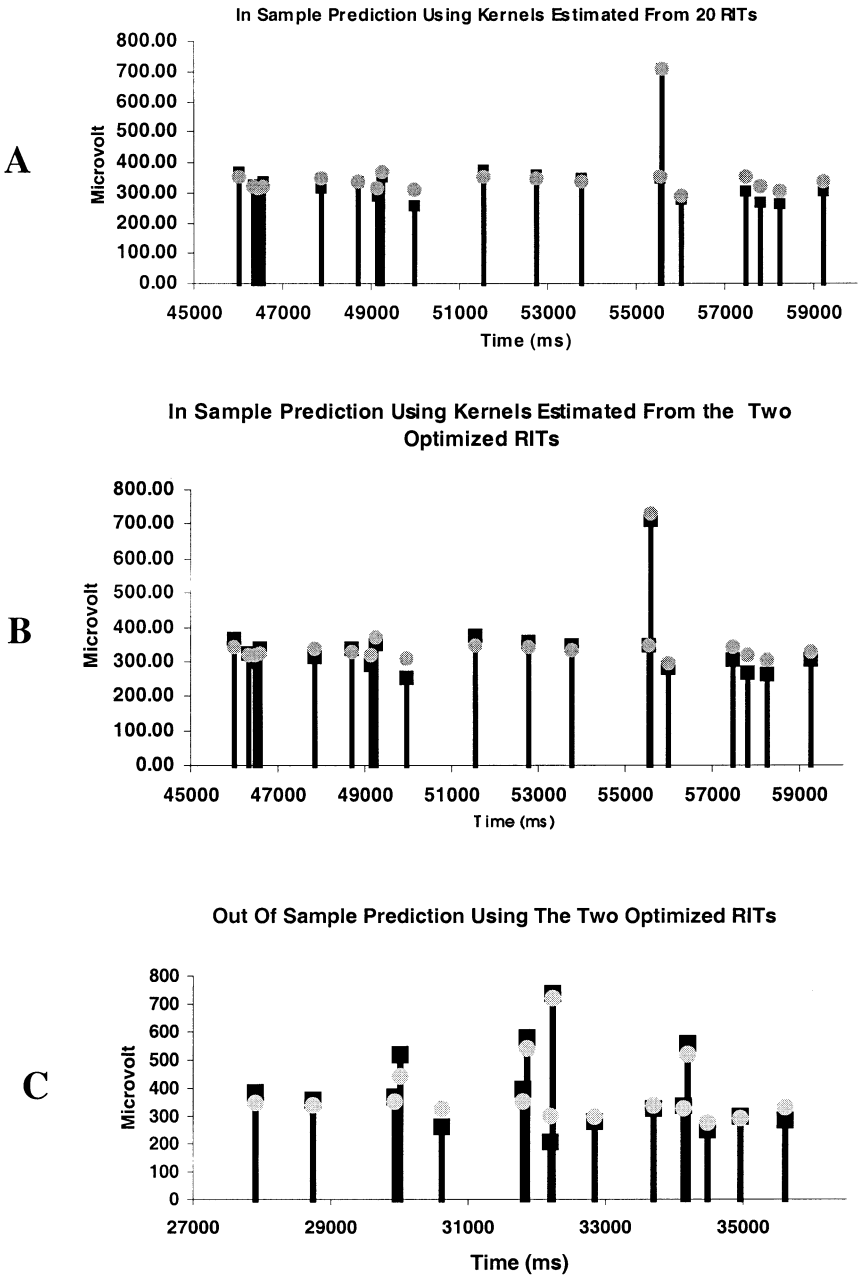

Fig. 12. Predictive power of kernels. (A) In-sample estimation, 20 RITs: a segment of population spike amplitudes (black squares) was taken from RIT #11. The predicted output (overlaid gray circles) was estimated using first- and second-order kernels that were calculated from all 20 input–output datasets. The NMSE value was 1.83%. (B) In-sample estimation, 2 RITs: the same data segment (black squares) shown in (A) is predicted using first- and second-order kernels estimated from the empirically optimized dataset corresponding to RITs #5 and #11 (gray circles). In this case, the NMSE value was 1.37%. Comparison between (A) and (B) and the associated NMSE values illustrates that, in our case, the two RITs (namely #5 and #11) were sufficient to provide a reliable model of the biological system. (C) Out-of-sample estimation, 2 RITs: a segment of real data that belonged to RIT #15 is shown using black squares. The predicted output (gray circles) was estimated using first- and second-order kernel estimates based on the datasets corresponding to RIT 5# and #11 datasets. Visual assessment and the NSME value of 4% illustrate the predictive power of the kernels.

with results reported in the literature (Alger and Teyler, 1976; Creager et al., 1980; Papatheodoropoulos and Kostopoulos, 2000). The predictions shown in Fig. 14 are based on computed kernels from RIT stimuli and have not been validated with data from impulse train experiments yet.

4.4. Results validation using the cross-correlation method

In order to establish continuity with previous work and compare it with the proposed method, estimation of the first- and second-order kernels was also performed using the cross-correlation method (Krausz and Friesen,

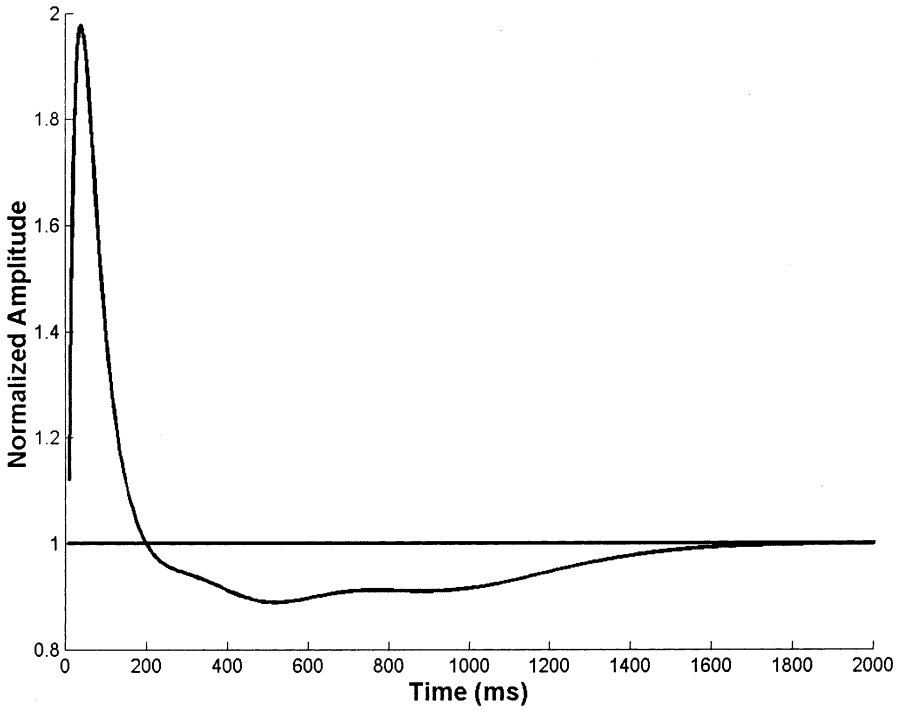

Fig. 13. Estimates of the conditioned response in impulse pair stimulation for interimpulse intervals varying from 0 to 2000 ms based on previously computed kernels and Eq. (3). The graph suggests facilitatory behavior for interimpulse intervals between 0 and 200 ms and inhibitory behavior for interimpulse intervals between 200 and 2000 ms.

1975; Berger et al., 1988a; Sclabassi et al., 1988). Kernels obtained using the cross-correlation method were compared with kernels obtained from the proposed method in terms of proximity of k_1 and k_2 values and prediction accuracy measured by the NMSE between the two methods.

Fig. 15A shows the second-order kernel obtained using the cross-correlation method (jagged line) and the proposed method (smooth line) for the same recording. The crosscorrelation method used all 20 RITs and 320 lags for the second-order kernel while the proposed method used only RITs #5 and #11. Smoothing the cross-correlation estimate with a triangular moving average window, we obtained the result shown in Fig. 15B. The NMSE for each case (3.83% for cross-correlation versus 3.60% for proposed method), the

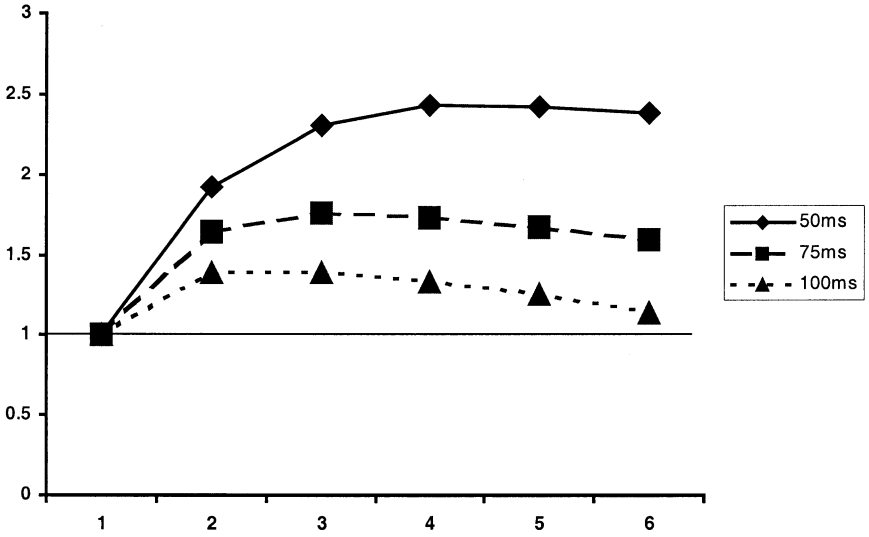

Fig. 14. Estimates of the amplitude of the population spike response to the 2nd, 3rd, 4th, 5th and 6th impulse of an impulse train stimulus for interimpulse intervals of 50, 75 and 100 ms. The graph suggests facilitatory behavior (population spike amplitudes greater than one), an observation consistent with results reported in the literature.

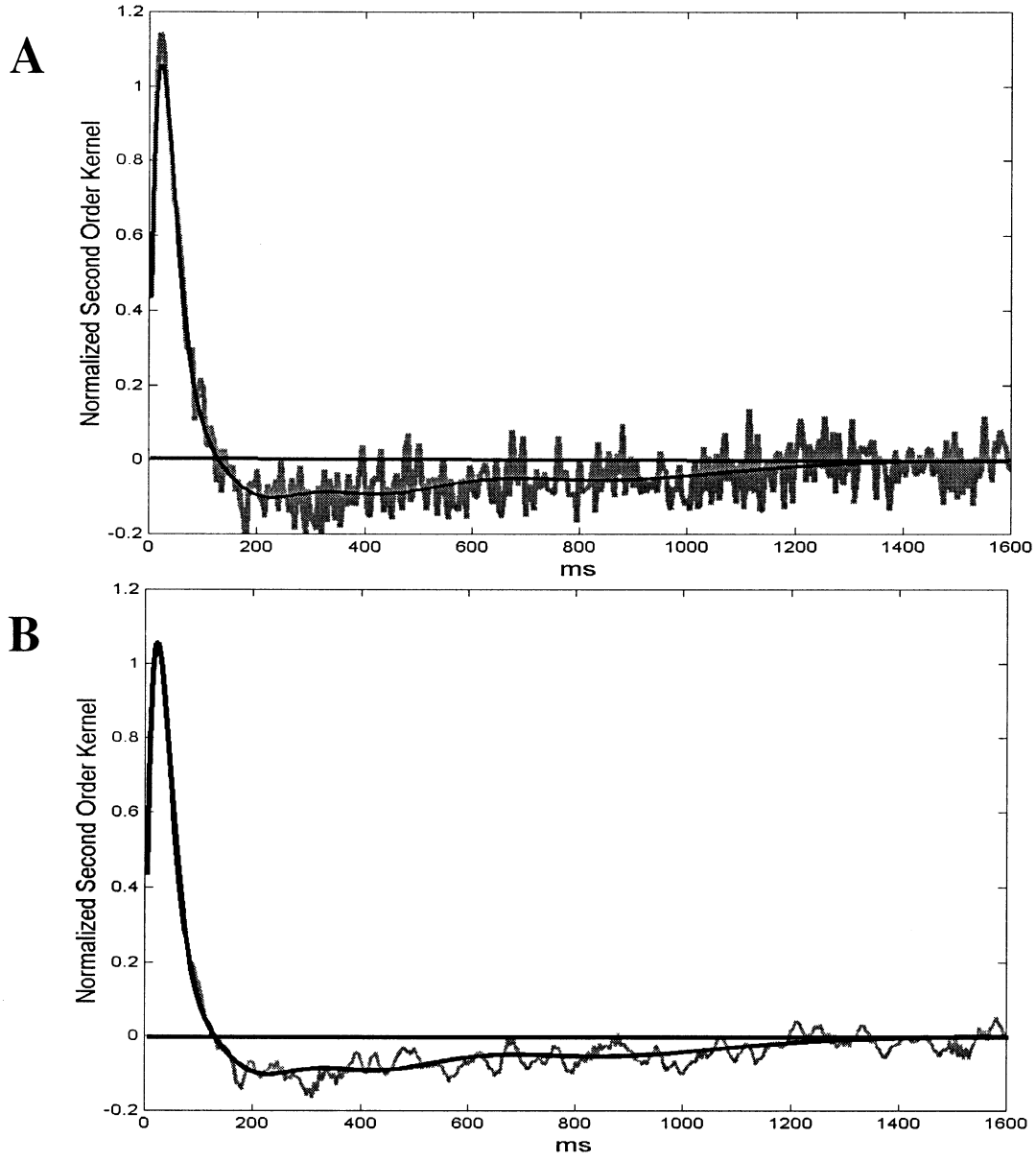

Fig. 15. Comparison of the second-order kernels obtained through cross-correlation method and the adapted Volterra–Wiener approach. (A) Second-order kernels obtained using the cross-correlation method (jagged line) and the adapted Volterra–Wiener method (smooth line) for the same recording. (B) Smoothing the cross-correlation estimate with a triangular moving average window yielded a relatively smoother curve. Visual comparison verifies the similarity of the second-order kernels from the two methods.

first-order kernel (345 μV for cross-correlation vs. 353 μV for proposed method), and the correlation coefficient (0.983) confirm that both methods yield comparable results.

Across all recordings, NMSE using the proposed method was 1% lower (on average) than NMSE using the crosscorrelation. The maximum difference of k_1 values between the two methods was within 10%, and the correlation coefficient between second-order kernels was 0.95 (S.D. $\pm$0.036). These results involved all 20 RITs and in-sample prediction. In the case that out-of-sample prediction and less than 20 RITs are considered, the proposed method offers an advantage in kernel estimation accuracy. This is illustrated in Fig. 16, where out-of-sample prediction NMSEs are plotted versus the number of RITs involved in estimating the kernels used for the prediction. In particular, prediction NMSEs for a RIT not included in the kernel estimation are shown. The top graph reports prediction NMSEs when the kernels are estimated with the cross-correlation method while the bottom graph reports NMSEs when the kernels are estimated with the proposed method. The advantage of the proposed method is reflected not only in the case-by-case (i.e. when 2, 4, 6, 8, 10, 12, 16 and 18 RITs were used to estimate the kernels) NMSE but also on the average as it is reflected by the corresponding

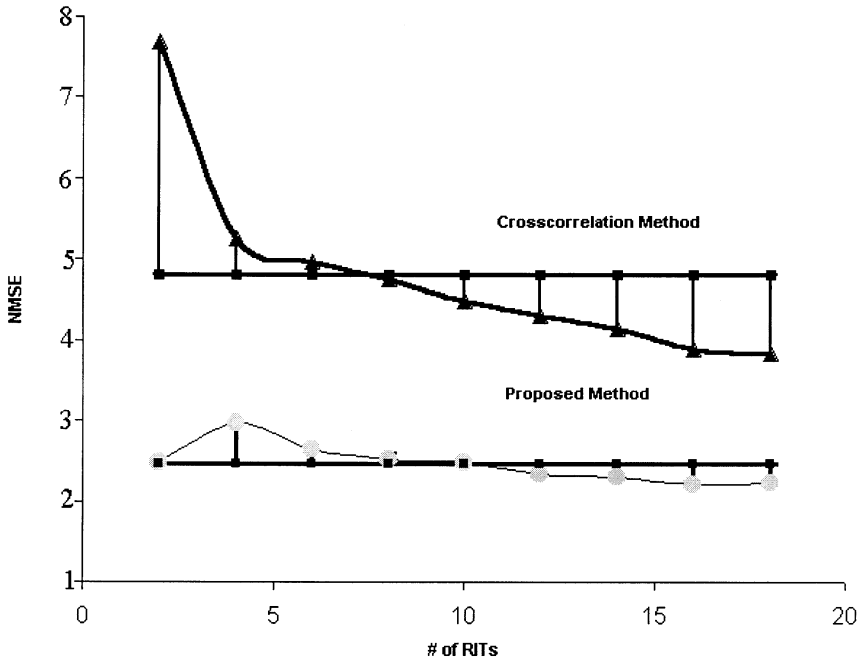

Fig. 16. Out-of-sample NMSE comparison between the proposed method and the crosscorrelation method versus the number of RITs employed for computing the kernels. The prediction NMSE for RIT #10 (out-of-sample RIT) from recording #6 (ordinate) is plotted vs. the number of RITs (other than RIT 10—in-sample RITs) used to estimate the kernels used for the prediction. The top graph shows NMSEs based on kernels estimated with the crosscorrelation method and bottom graph shows NMSEs based on the proposed method. Both graphs are showing the mean NMSE value for each kernel estimation approach across all cases (2, 4, 6, 8, 10, 12, 14, 16 and 18 RITs) and the deviation from the mean for each case.

mean NMSE values for each approach (i.e. 4.68% for the crosscorrelation method versus 2.87% for the proposed method). Note, that the largest difference in NMSE between the two methods occurs when only two RITs are used (7.51% for the crosscorrelation method versus 2.87% for the proposed method). This is typical because short data records have a significant effect on the variability of the kernel estimates, when the cross-correlation method is used.

5. Discussion

Traditionally, STP has been characterized using paired pulse stimuli with variable interimpulse intervals and impulse train stimuli with fixed interimpulse intervals. We have generalized STP characterization in several respects by: (1) introducing impulse sequence stimuli of randomly varying interimpulse interval; (2) considering the amplitudes of the corresponding population spike response sequences; and (3) introducing quantitative STP descriptors and a mathematical model of STP with predictive capabilities.

The introduction of stimuli sequences of randomly variable interimpulse intervals, combined the variability of interimpulse intervals in paired pulse experiments with the impulse succession feature in impulse trains. This innovative approach considerably reduced experimental time, especially when it was coupled with the empirical optimization (shortening the length) of the stimulus sequence. The reduction in stimulus duration was by a factor of 10, decreasing the number of required impulses from 4000 to 400. The consideration of the effect of interimpulse intervals on the amplitude of the population spikes formed an approach consistent with the paired pulse and the impulse train methods. The quantitative STP descriptors (kernels) presented a comprehensive picture of excitatory and inhibitory STP behavior depending on interimpulse intervals. These quantitative descriptors were sufficient to capture the behavior of the nonlinear dynamic mechanisms underlying STP in this area of the hippocampus, although the residual NMSE suggested that a third-order kernel may be plausible. In addition to describing STP nonlinear dynamics, the kernels offered predictive capabilities when used in conjunction with the model of Eq. (1). Such STP models help in evaluating the accuracy of the STP descriptors via the output prediction error and provide the capability of predicting responses to arbitrary input patterns.

The characterization of STP, using the new approach presented in this article, required significantly reduced data collection time and employed computationally efficient data analysis methods. These computational methods can be readily extended to include population spike latencies and can be adapted to the analysis of dendritic and somatic EPSP data. We are planning to apply this new approach to the characterization of STP

in the CA1 region before and after drug delivery and use the STP descriptors presented in this article to assess drug effects.

Acknowledgements

This work was supported by grant no. RR-01861 from the Division of Research Resources of the National Institutes of Health and by grants 0646 and 0259 from DARPA Controlled Biological Systems Program and the Office of Naval Research.

References

Abbot LF, Varela JA, Sen K, Nelson SB. Synaptic depression and cortical gain control. Science 1997;275:220–4.

Alberston TE, Walby WF, Stark LG, Joy RM. The effect of propofol on the CA1 pyramidal cell excitability and GABA-A mediated inhibition in the rat hippocampal slice. Life Sci 1996;58(26):2397–407.

Alger BE, Teyler TJ. Long-term and short-term plasticity in the CA1, CA3, and dentate regions of the rat hippocampal slice. Brain Res 1976;110(3):463–80.

Andersen P, Bliss TVP, Skrede KK. Lamellar organization of hippocampal excitatory pathways. Exp Brain Res 1971;13:208–11.

Berger TW, Eriksson JL, Ciarolla DA, Sclabassi RJ. Nonlinear systems analysis of the hippocampal perforant path-dentate projection. II. Effects of random train stimulation. J Neurophysiol 1988a;60:1077–94.

Berger TW, Eriksson JL, Ciarolla DA, Sclabassi RJ. Nonlinear systems analysis of the hippocampal perforant path-dentate projection. III. Comparison of random train and paired impulse stimulation. J Neurophysiol 1988b;60:1095–109.

Berger TW, Harty TP, Barrionuevo G, Sclabassi RJ. Modeling of neuronal networks through experimental decomposition. In: Marmarelis VZ, editor. Advanced methods of physiological system modeling, vol. II. New York: Plenum, 1989:113–28.

Bliss TVP, Lomo T. Long-lasting potentiation of synaptic transmission in the dentate area of the anaesthetized rabbit following stimulation of the perforant path. J Neurophysiol 1973;232:331–56.

Colmers WF, Lukowiak K, Pittman QJ. Neuropeptide Y reduces orthidromically evoked population spike in rat hippocampal CA1 by a possibly presynaptic mechanism. Brain Res 1985;346(2):404–8.

Courellis SH, Marmarelis VZ, Berger TW. Modeling event-driven nonlinear dynamics, in: Biological Neural Networks, Proceedings of the 7th Joint Symposium on Neural Computation 2000;10:28–35.

Creager R, Dunwiddie T, Lynch G. Paired-pulse and frequency facilitation in the CA1 region of the in vitro rat hippocampus. J Neurophysiol 1980;299:409–24.

Dobrunz LE, Huang EP, Stevens CF. Very short-term plasticity in hippocampal synapses. Proc Natl Acad Sci USA 1997;94:14843–7.

Fueta Y, Ohno K, Mita T. Large frequency potentiation induced by 2 Hz stimulation in the hippocampus of epileptic El mice. Brain Res 1998;792(1):79–88.

Gross GW, Rhoadas BK, Reust DL, Schwalm FU. Stimulation of monolayer networks in culture through thin film indium-tin oxide recording electrodes. J Neurosci Methods 1993;50:131–43.

Harris KM, Teyler TJ. Age differences in a circadian influence on hippocampal LTP. Brain Res 1983;261(1):69–73.

Harris EW, Ganong AH, Cotman CW. Long-term potentiation in the hippocampus involves activation of *N*-methyl-D-aspartate receptors. Brain Res 1984;323(1):132–7.

Krausz HI, Friesen WO. Identification of nonlinear systems using random impulse train inputs. Biol Cybern 1975;19:217–30.

Krugers HJ, Mulder M, Korf J, Havekes L, DeKloet ER, Joels M. Altered synaptic plasticity in hippocampal CA1 area of apolipoprotein E deficient mice. Neuroreport 1997;8(11):2505–10.

Landfield PW, Pitler TA, Applegate MD. The effects of high Mg^{2+}-to-Ca^{2+} ratios on frequency potentiation in hippocampal slices of young and aged rats. J Neurophysiol 1986;56(3):797–811.

Leung LS, Fu XW. Factors affecting paired-pulse facilitation in the hippocampal CA1 neurons in vitro. Brain Res 1994;650:75–84.

Marmarelis VZ. Identification of nonlinear biological systems using Laguerre expansions of kernels. Ann Biom Eng 1993;21:573–89.

Nelson TE, Ur CL, Gruol DL. Chronic intermittent ethanol exposure alters CA1 synaptic transmission in rat hippocampal slices. Neurosci 1999;94(2):431–42.

Pananceau M, Chen H, Gustafsson B. Short-term facilitation evoked during brief afferent tetani is not altered by long-term potentiation in the guinea-pig hippocampal CA1 region. J Physiol 1998;508(2):503–14.

Papatheodoropoulos C, Kostopoulos G. Dorsal-ventral differentiation of short-term synaptic plasticity in rat CA1 hippocampal region. Neurosci Lett 2000;286(1):57–60.

Perrett S, Dudek S, Eagleman D, Montague P, Friedlander M. LTD induction in adult visual cortex: role of stimulus timing and inhibition. J Neurosci 2001;21(7):2308–19.

Sclabassi RJ, Eriksson JL, Port R, Robinson G, Berger TW. Nonlinear systems analysis of the hippocampal perforant path-dentate projection I. Theoretical and interpretational considerations. J Neurophysiol 1988;60:1066–76.

Stanford IM, Wheal HV, Chad JE. Bicuculline enhances the late GabaB receptor-mediated paired pulse inhibition observed in the rat hippocampal slices. Eur J Pharmacol 1995;277(2–3):229–34.

Turner RW, Miller JJ. Effects of extracellular calcium on low frequency induced potentiation and habituation in the in vitro hippocampal slice preparation. Can J Physiol Pharmacol 1982;60(3):266–7.

Wheal HV, Lancaster B, Bliss TV. Long-term potentiation in Schaffer collateral and commissural systems of the hippocampus: in vitro study in rats pretreated with kainic acid. Brain Res 1983;272(2):247–53.

Yamamoto C, Matsumoto K, Takagi M. Potentiation of excitatory postsynaptic potentials during and after repetitive stimulation in thin hippocampal sections. Exp Brain Res 1980;38(4):469–77.

Wiener N. Nonlinear problems in random theory. New York: The Technology Press of MIT and Wiley, 1958.